Characterization of atmospheric muons at sea level using a cosmic ray telescope

Jean-Luc Autran, Daniela Munteanu, Tarek Saad Saoud, Soilihi Moindjie

▶ **To cite this version:**

Jean-Luc Autran, Daniela Munteanu, Tarek Saad Saoud, Soilihi Moindjie. Characterization of atmospheric muons at sea level using a cosmic ray telescope. Nuclear Instruments and Methods in Physics Research Section A: Accelerators, Spectrometers, Detectors and Associated Equipment, 2018, 903, pp.77-84. 10.1016/j.nima.2018.06.038 . hal-01846825

HAL Id: hal-01846825
https://hal.science/hal-01846825v1

Submitted on 2 Apr 2019

HAL is a multi-disciplinary open access archive for the deposit and dissemination of scientific research documents, whether they are published or not. The documents may come from teaching and research institutions in France or abroad, or from public or private research centers.

L'archive ouverte pluridisciplinaire **HAL**, est destinée au dépôt et à la diffusion de documents scientifiques de niveau recherche, publiés ou non, émanant des établissements d'enseignement et de recherche français ou étrangers, des laboratoires publics ou privés.

Characterization of Atmospheric Muons at Sea Level Using a Cosmic Ray Telescope

J.L. Autran*, D. Munteanu, T. Saad Saoud, S. Moindjie

Aix-Marseille Univ, Univ Toulon and CNRS, IM2NP UMR 7334

Faculté des Sciences, Service 142, Avenue Escadrille Normandie Niémen

F-13397 Marseille Cedex 20, France

Abstract

In this work, a portable cosmic-ray telescope was designed, assembled and operated to measure the cosmic-ray induced atmospheric muon flux at ground level. The instrument was entirely characterized and modeled from the point-of-view of detector efficiency, energy detection window and counting rate. Experimental data are reported for the characterization of the muon flux at sea level (43°N of latitude) in terms of vertical muon intensity and zenithal angle dependence.

Keywords: Atmospheric muons, cosmic rays, muon flux, muon telescope, sea level muon intensity, zenithal angle distribution

*Corresponding author. Tel: + 33 413594627, fax: +33 491288531

E-mail address: jean-luc.autran@univ-amu.fr

1. Introduction

A large number of experimental works has been reported in the last decades on cosmic-rays muon intensities at sea level; these data are important for astrophysical standards and contain useful information concerning cosmic-ray interaction processes [1]. In a completely different field of interest, that initially motivated the present work, the metrology of terrestrial cosmic rays is also an essential challenge in modern microelectronics, for the understanding of basic mechanisms and for the characterization, modeling and predictive simulation of single event effects (SEE) in electronics [2]. SEE are radiation-induced errors in microelectronic circuits caused when energetic particles lose energy by directly (charged particles) or indirectly (neutrons) ionizing the medium through which they pass, creating electron-hole pairs at the origin of transient parasitic currents [3]. If the effort has so far focused mainly on the characterization of atmospheric neutrons [4-8], one must not longer neglect muons at ground level that are susceptible to significantly contribute to SEE in current integrated electronics [9-12]. Muons are indeed the most numerous energetic charged particles at sea level. They arrive at sea level with an average flux of about 1 muon per square centimeter and per minute. Their mean energy at sea level is ~4 GeV. For these typical energies and up to a few hundred of GeV, muons mainly interact with matter by ionization, losing energy at a fairly constant rate of about 2 MeV per g/cm^2. Although a large literature exists on muons in the atmosphere, studies are generally oriented “high energy physics” and consider muon energies above the GeV or beyond [11]. In the particular framework of radiation effects in microelectronics, there is an evident lack of data available in the “low energy” range, typically above a few tens of MeV and below a few GeVs. At these energies, muons can easily penetrate packaged ICs but are rapidly slowed or stopped: they can deposit by ionization a significant amount of electric charge along their track and contribute to single-event effects.

In the present work, we developed a cosmic-ray telescope to accurately characterize, in a long-term perspective effort, the atmospheric muon flux at ground level, precisely in this "low energy" range. This paper presents and discusses in details the main characteristics of the instrument and reports the experimental measurements conducted in the region of Marseille (south of France) at sea level.

2. The muon telescope

2.1. Experimental setup

In this work, we developed an experimental apparatus called "cosmic-ray telescope". Figure 1 shows the front and back views of this setup derived from a real astronomical telescope fabricated by SkyVision (ultra compact Dobson, model 400-UT [13]). The initial telescope has been modified to receive two circular plastic scintillators (diameter 40 cm, thickness 5 cm, housed in 1.5 mm of aluminum plate) in place of the classical primary and secondary optical mirrors. This solution offers the advantage to take full benefits from an alt-azimuthal PC-controlled motorized mount with high precision mechanics and great transportability. The polymer base material of the two detectors is polyvinyltoluene (PVT) fabricated by Eljen Technology (EJ-200) [14]. This plastic is highly sensitive to charged particles: its typical stopping power for 1 GeV muons is 2.132 MeV/cm [15]. The two scintillators have photomultipliers (PM) directly integrated in their volume and optically coupled using a high refractive index optical coupling medium. The PMs are ADIT model PB29 with 1.125" diameter, 2π photocathode and 11-stage photomultiplier. The assembly (PM+scintillator) is mounted in an aluminum housing (thickness 1.5 mm) that ensures a permanent light sealing. The two PMs are connected to the measurement and acquisition chain shown in Figure 2.

The electronics chain trigs the muons traversing the front scintillator and measures, using a coincidence detection procedure, their time-of-flight between the front and back detectors

80 separated by a distance of 1.02 m (in air). PM signals as well as time-of-flights converted in
81 voltage pulses using a time-to-amplitude converter (TAC) are digitalized using multi-channel
82 analyzers (MCAs based on 16k ADCs).

83 *2.2. Instrument calibration*

84 In order to be sure that the telescope detects and counts only atmospheric muons, a careful
85 characterization and calibration of the instrument has been performed in several steps,
86 described below.

87 *2.2.1. Single detector characterization and γ rays rejection*

88 In addition to muons, the two scintillators coupled with PMs of the telescope detect gamma
89 rays, which are particularly present at low incident energy. Figure 3 shows the telescope
90 counting rate as a function of the MCA channel number. This curve shows two peaks: (i) a
91 first low-energy peak that consists of a mixture of PM noise and the contribution of ambient
92 gamma radiation; (ii) a second peak corresponding to the contribution of charged atmospheric
93 muons. Note that the integral of this second peak (1200 to 1300 counts/min) corresponds
94 perfectly to the product of the surface of the detector (1256 cm^2 in this case) with the
95 integrated average muon flux at ground level (about 60 muons per square centimeter and per
96 hour), demonstrating that this second peak is due almost exclusively to the contribution of
97 muons in the count rate. In order to minimize the influence of gamma rays in measurements, a
98 detection threshold of approximately 130 mV (corresponding to ADC channel 3500) was
99 considered, as shown schematically in Figure 3. Since this threshold is very dependent on the
100 PM tube, a threshold value has been separately determined for each of the two (front and
101 back) telescope detectors.

102 *2.2.2. Detector efficiency*

103 The raw counting rate of the telescope needs to be corrected to take into account the detection
104 efficiency of both front and back detectors since these sometimes do not detect a passing

105 muon. For each detector, the detection efficiency is obtained by calculating the ratio between
106 the number of detected particles and the number of incident particles effectively passing
107 thought the bulk scintillator. To do this, we performed a coincidence measurement using three
108 stacked detectors, as shown in the diagram of Figure 4 (top). The detector #2 to be
109 characterized is placed between two other detectors (#1 and #3) and the system measures,
110 over a certain time interval, the number of events detected in coincidence, CR_{13}, between the
111 detectors #1 and #3. Thus, if a muon is detected by #1 and #3 in coincidence, it has
112 necessarily crossed the scintillator #2. At the same time, the system therefore measures the
113 number of coincidences, CR_{123}, between detectors #1, #2 and #3. The efficiency of the
114 detector to be characterized, η_2, is therefore given by:

115 $$\eta_2 = CR_{123}/CR_{13} \quad (1)$$

116 The efficiency of the two detectors of the telescope was estimated using this procedure.
117 Figure 4 (bottom) shows the variation with time of CR_{13}, CR_{123} and η_2 for the front detector.
118 From these results, the measured detection efficiency of the telescope was estimated at
119 η_F = 95.8 % and η_B = 96.0 % for the front and back detectors respectively (Figure 4). The
120 measured values remain constant over time, as shown in Figure 4 for the front detector, and
121 have been taken into account in the correction of all the experimental results.

122 *2.2.3. Electronic chain calibration*

123 A calibration procedure has been preliminary performed to determine the MCA channel
124 number versus time proportionality. The MCA was calibrated to a resolution of
125 approximately 160 bins/ns. From time-of-flight distributions (not shown) of incident muons
126 in the vertical direction for two detector distances of 25.5 cm and 104 cm, we deduced the
127 average speed of cosmic ray muons, v_μ = 29.5 ± 2.1 cm/ns, i.e. 98.4% of c, in perfect
128 agreement with the accepted value of 0.98×c [15].

129

130 *2.3. Telescope modeling and simulation*

131 *2.3.1. TRIM simulation*

132 In order to determine the minimum energy of muons that can be detected by the telescope, we
133 performed extensive simulations using the TRIM (Transport of Ions in Matter) Monte Carlo
134 simulation code [16]. In these simulations, we considered the exact 1D stack of materials
135 traversed by incident muons during their passage through the instrument. Muons have been
136 emulated in TRIM by applying a simple "mass scaling" to protons, as suggested in [17].
137 Figure 5 shows the average distance traversed by muons in the instrument (perpendicular
138 tracks) as a function of their incident energy. If muons with incident energies up to about 33
139 MeV are stopped in the front detector, higher energetic particles can reach the back detector
140 and completely cross it above 50 MeV. Estimating that a particle depositing around 2 MeV in
141 the scintillator material can be detected by the PM, the setup is thus able to detect incident
142 muons above E_{min} = 38 MeV, which corresponds to the low energy cut-off of the instrument
143 for particle tracks perpendicular to the detector. This value should be slightly higher for
144 oblique tracks.

145 *2.3.2. Counting rate modeling of the telescope*

146 In a second step, the telescope counting rate has been numerically estimated from a model
147 directly derived from the work of Sanderson and Page [18] in the case where the telescope is
148 rotating under an anisotropic distribution of particles. Figure 6 introduces the notations used
149 in the following.

150 For an anisotropic distribution of incident muons I ($m^{-2}s^{-1}sr^{-1}$), the counting rate CR (s^{-1}) of
151 the telescope pointing in the zenithal direction θ_d can be expressed as [18]:

152 $$\mathrm{CR}(\theta_d) = \eta_F \eta_B \int_0^{\Phi_m} \int_0^{\theta_m} S(\theta) I(\theta, \Phi) \sin\theta \cos\theta d\theta d\Phi \quad (2)$$

where η_F and η_B are the front and back detector efficiencies, respectively, θ_m is the acceptance angle of the telescope, S is the intersection of the projected shadow area of the front detector within the plane surface of the second detector [19] and Φ_m is the maximum value of the azimuthal angle for counting particles coming from the upper hemisphere [18]. $\Phi_m = 2\pi$ for a telescope pointing vertically ($\theta_d = 0$). For $\theta_d > 0$ and if $\theta + \theta_d > \pi/2$, the integration over Φ must be stopped at the angle Φ' where Φ' is given by:

$$\Phi' = \frac{\pi}{2} + sin^{-1}(cot\theta cot\theta_d) \quad (3)$$

For a cylindrically telescope with two parallel and circular detectors of same radius R separated by the distance ℓ, as represented in Figure 7, the intersection surface S (cross-hatched area) is given by Thomas and Willis [19]:

$$S(\theta) = 2R^2\, arccos\left(\frac{\ell \tan\theta}{2R}\right) - \ell \tan\theta \sqrt{R^2 - \left(\frac{\ell \tan\theta}{2}\right)^2} \quad (4)$$

If we suppose in addition that the muon flux intensity susceptible to be detected by the telescope ($E_{min} > 38$ MeV) in a given arbitrary direction (vector OB, see Fig. 6) only depends on the zenithal angle θ' following a power cosine law, we can write:

$$I(\theta') = I_0 cos^n(\theta') \quad (5)$$

where I_0 is the vertical muon flux (expressed in $m^{-2}.s^{-1}.sr^{-1}$) in the reference direction of the muon distribution (vector OA, see Fig. 6) and n is a real parameter.

In the general case depicted in Figure 6, the angle between vectors OA and OB (an arbitrary vector) is [16]:

$$cos\theta' = cos\theta cos\theta_d + sin\theta sin\theta_d cos\phi \quad (6)$$

175 Eq. (5) reduces to θ′ = θ when the telescope is pointing vertically (in this case, the z-axis
176 attached to the telescope coincides to the reference direction OA of the muon distribution). In
177 this particular case only, Eq. (2) reduces to [18,20]:

178 $$\mathrm{CR}^{V}(\theta_d) = 2\pi \times \eta_F \eta_B \int_0^{\theta_m} S(\theta) I(\theta) \sin\theta \cos\theta d\theta \qquad (7)$$

179 where CR^{V} (s^{-1}) is the vertical counting rate of the telescope.

180

181 The numerical integration of Eq. (2) using Eqs. (3) to (6) over the acceptance angle of the
182 telescope allows us to estimate the telescope counting rate in the zenithal direction θ_d for any
183 given values of I_0 and n, the two unknown quantities of this set of equations.

184

185 **3. Experimental results: sea level measurements**

186 Measurements have been performed outdoors on the Aix-Marseille University campus of
187 Saint-Jérôme (Marseille, France, +43.338°N, +5.412°E, altitude 118 m) and on the roof of the
188 Cassis's conference center (Cassis, France, +43.213°, +5.537°E, altitude 7 m). For the two
189 measurement locations, the telescope was installed on a horizontal concrete slab during non-
190 rainy days (Figure 8 left). A control software has been developed to automatically perform the
191 complete scanning over the solid angle (2π) or a partial scanning for fixed azimuthal or
192 zenithal angle. The software also controls the integration time, timestamps all measurements
193 and transfer data on the laboratory server for post-treatment.
194 To obtain additional values of the vertical counting rate as a function of the separation
195 distance between the front and back detectors, a plastic resin shelf with seven regularly
196 spaced shelves was also used in place of the telescope setup (Figure 8 right). In this case, the
197 two detectors were temporarily removed from the telescope bracket and aligned vertically on
198 two shelves of this complementary characterization setup.

199 *3.1. Vertical muon intensity*

200 Measurements have been firstly performed with the telescope pointed in the vertical direction.
201 A stable counting rate of 78 counts/min was measured over several days. Considering the
202 acceptance angle of the instrument defined in Figure 6 (θ_m = 19,335°), this counting rate
203 roughly corresponds to a vertical muon intensity $I_0 \approx 100$ $m^{-2}.s^{-1}.sr^{-1}$, in very good agreement
204 with vertical flux values reported in literature at this latitude for energy muons ~3GeV [1, 20].
205 To check the validity of the telescope counting rate model described in paragraph 2.3.2 (Eq.
206 (7)), we performed measurements in the vertical direction as a function of the separation
207 distance between the front and back detectors using the additional setup (plastic shelf)
208 described above. Figure 9 shows the results of the model characterization: the values
209 (represented in both linear and semi-logarithm scales) are in very good agreement in a
210 distance range between 10 cm and 2 m with the results of simulation using the numerical
211 model presented above (Eq. (7) with n =2 and $I_0 = 100$ $m^{-2}.s^{-1}.sr^{-1}$, see section 3.2).

212 *3.2. Angular distribution of muons*

213 Figures 10 shows the variation of the muon flux with the zenithal angle of the telescope. Each
214 point corresponds to a value averaged over one hour. These raw measurements are well-fitted
215 by a cosine power law with n = 2.0 ± 0. This value is in excellent agreement with the value
216 generally reported in the literature also for energy muons ~ 3 GeV [1, 21].
217 If we consider now the numerical model developed in section 2.3.2 (Equations (2) to (6)), this
218 model also perfectly fits experimental values of Figure 10 when tuning I_0 and n parameters
219 respectively to values $I_0 = 100$ $m^{-2}.s^{-1}.sr^{-1}$ and n = 2.0. Additional curves in Figure 10
220 calculated for n = 1.9 and n = 2.1 are also plotted (always for $I_0 = 100$ $m^{-2}.s^{-1}.sr^{-1}$). These
221 curves graphically illustrated the sensitivity of the model to this parameter and allow us to
222 roughly estimate the uncertainty on the determination of n = 2.0 ± 0.1.

223 *3.3. Measurements over the hemisphere*

Figure 11 shows the averaged values of the telescope counting rate as a function of both zenithal and azimuthal angles. Each point corresponds to a value averaged over one hour: the total acquisition time for these measurements is 72 h. No significant asymmetry of the muon flux distribution with respect to the azimuthal direction is observed for such a relatively short acquisition time of one hour per point.

From the angular distribution of Figure 11, the integral flux of atmospheric muons over the hemisphere (solid angle 2π) has been evaluated to 209.4 $cm^{-2}s^{-1}$, that corresponds to ~1.26 $m^{-2}min^{-1}$.

5. Conclusion

In this paper we presented a muon telescope developed in this work to accurately characterize the flux of atmospheric muons at ground level as a function of both zenithal and azimuthal angles. The experimental setup, the control software and the calibration of the instrument have been described in detail. Through TRIM simulation work we have established that the telescope can detect incident muons with a minimum energy of 38 MeV in vertical incidence. We also presented a modeling of the counting rate of the telescope based on a model published in the literature. Our experimental measurements showed that the muon intensity in vertical incidence is $I_0 \approx 100$ $m^{-2}.s^{-1}.sr^{-1}$, in very good agreement with the values of the vertical flux reported in literature at this latitude. Then, we have finely characterized the dependence of atmospheric muon flux with the zenithal angle of the telescope and with the azimuthal direction. Raw measurements as well as the fitting of our model on experimental data showed a perfect square cosine dependence ($n = 2.0 \pm 0.1$) of the incident muon distribution, in excellent agreement with the value generally reported in the literature for energy muons ~3 GeV.

Acknowledgments

This work has been conjointly supported by France's General Directorates DGA and DGE, under convention #132906128 (EVEREST project).

References

[1] P.K.F. Grieder, Cosmic Rays at Earth, Elsevier Press, Netherlands, 2001.

[2] J.L. Autran and D. Munteanu, Soft Errors: from particles to circuits, Taylor & Francis/CRC Press, 439 p., 2015.

[3] D. Munteanu and J.L. Autran, "Modeling and Simulation of Single-Event Effects in Digital Devices and ICs", IEEE Trans. Nucl. Sci., vol. 55, no. 4, pp. 1854-1878, 2008.

[4] S. Semikh, S. Serre, J.L. Autran, D. Munteanu, S. Sauze, E. Yakushev, S. Rozov, "The Plateau de Bure Neutron Monitor: Design, Operation and Monte-Carlo Simulation", IEEE Trans. Nucl. Sci., vol. 59, no. 2, pp. 303-313, 2012.

[5] J.L. Autran, D. Munteanu, P. Roche, G. Gasiot, S. Martinie, S. Uznanski, S. Sauze, S. Semikh, E. Yakushev, S. Rozov, P. Loaiza, G. Warot, M. Zampaolo, "Soft-errors induced by terrestrial neutrons and natural alpha-particle emitters in advanced memory circuits at ground level", Microelectronics Reliability, vol. 50, pp. 1822–1831, 2010.

[6] J.L. Leray, "Effects of atmospheric neutrons on devices, at sea level and in avionics embedded systems", Microelectronics Reliability, vol. 47, pp. 1827–1835, 2007.

[7] J.L. Autran, S. Serre, D. Munteanu, S. Martinie, S. Sauze, S. Uznanski, G. Gasiot, P. Roche, "Real-Time Soft-Error Testing of 40nm SRAMs", 2012 Proceeding of the IEEE International Reliability Physics Symposium (IRPS), pp. 3C.5.1-3C.5.9, 2012.

[8] J.L. Autran, D. Munteanu, P. Roche, G. Gasiot, "Real-Time Soft-Error Rate Measurements: a Review", Microelectronics Reliability, vol. 54, pp. 1455-1476, 2014.

[9] B.D. Sierawski, M.H. Mendenhall, R.A. Reed, M.A. Clemens, R.A. Weller, R.D. Schrimpf, E.W. Blackmore, M. Trinczek, B. Hitti, J.A. Pellish, R.C. Baumann, S.-J. Wen, R. Wong, N. Tam, "Muon-Induced Single Event Upsets in Deep-Submicron Technology", IEEE Trans. Nucl. Sci., vol. 57, no. 6, pp. 3273 - 3278, 2010.

[10] B.D. Sierawski, R.A. Reed, M.H. Mendenhall, R.A. Weller, R.D. Schrimpf, S.-J. Wen, R. Wong, N. Tam, R.C. Baumann, “Effects of Scaling on Muon-Induced Soft Errors”, 2011 Proceeding of the IEEE International Reliability Physics Symposium (IRPS), 2011.

[11] L.W. Massengill, B.L. Bhuva, W.T. Holman, M.L. Alles, T.D. Loveless, “Technology Scaling and Soft Error Reliability”, 2012 Proceeding of the IEEE Reliability Physics Symposium (IRPS), pp. 3C.1.1-3C.1.7, 2012.

[12] P. Roche, J.L. Autran, G. Gasiot, D. Munteanu, “Technology downscaling worsening radiation effects in bulk: SOI to the rescue”, IEEE International Electron Device Meeting (IEDM), pp. 766-769, 2013.

[13] https://skyvision.fr/the-user-guide/dobson/ultra-compact-dobson/?lang=en

[14] http://www.eljentechnology.com/index.php/component/content/article/31-general/48-ej-200

[15] D.E. Groom, et al., Atomic Data and Nuclear Data Tables 78, pp. 183-356, 2001.

[16] J.F. Ziegler, J.P. Biersack, U. Littmark. The Stopping and Range of Ions in Matter. Pergamon, New York, 1985.

[17] H.H.K. Tang, “SEMM-2: A new generation of single-event-effect modeling tools,” IBM Journal of Research and Development, Vol. 52, pp. 233-244, 2008.

[18] T.R. Sanderson, D.E. Page, “Geometrical aspects of the performance of cosmic ray detector telescopes in non-isotropic particle distributions”, Nuclear Instruments and Methods, Volume 104, Issue 3, pp. 493-504, 1972.

[19] G.R. Thomas and D.M. Willis, “Analytical derivation of the geometric factor of a particle detector having circular or rectangular geometry”, Journal of Physics E: Scientific Instruments, Vol. 5, N°3, p. 261-263, 1971.

[20] J.D. Sullivan, “Geometrical factor and directional response of single and multi-element particle telescopes”, Nuclear Instruments and Methods, Vol. 95, p. 5-11, 1971.

[21] S. Cecchini, M. Spurio, “Atmospheric muons: experimental aspects”, Geosci. Instrum. Method. Data Syst., Vol. 1, p. 185-196, 2012.

Table and figure captions

Figure 1. Front and back views of the portable experimental setup (total weight 48 kg) composed of two circular scintillators (400 mm diameter) mounted in place of the primary and secondary mirrors of a real astronomical telescope with an alt-azimuthal double-axis motorized mount. The distance between the two scintillators is 102 cm.

Figure 2. Schematics of the electronics acquisition chain for measuring the time-of-flight of coincidence muons between the two detectors of the telescope.

Figure 3. Single detector acquisition chain used for fine-tuning the discrimination threshold in order to reject the gamma ray background. After threshold calibration, the counting rate of a single horizontal detector is 1200-1300 counts/min, that corresponds to approximately 60 particles per cm^2 and per hour.

Figure 4. Schematics of the electronics acquisition chain for measuring the detector efficiency. The detector to characterize (#2) is surrounded by two additional detectors (#1 and #3) used to count muons traversing the detector stack with and without the contribution of detector #2 in the coincidence counting rates, respectively noted CR_{123} and CR_{13}.

Figure 5. TRIM simulations showing the slowing and stopping of muons in the telescope as a function of their incident energy (particle tracks perpendicular to the detector surfaces).

Figure 6. Definition of axes, angles and other quantities used for the evaluation of the telescope counting rate when the distribution is rotated about the instrument. (Ox, Oy, Oz) is

fixed with respect to the detector, OA is the reference direction of the muon distribution (vertical direction of the site), and OB is an arbitrary vector. For the instrument, the acceptance angle is θ_m = 19°335.

Figure 7. Geometrical model used to derivate Eq. (2) from the "shadow area" approach described in Ref. [19].

Figure 8. (left) The muon telescope outdoors in Cassis (France) at sea level; (right) An additional setup based on a plastic resin shelf used to characterize the counting rate in the vertical direction as a function of the distance between the two detectors.

Figure 9. Counting rate in the vertical direction as a function of the separation distance between the front and back detectors using the additional setup (plastic shelf) described in Figure 8. The experimental points labeled "telescope" correspond to values measured using the telescope setup (distance of 1.02 m between the detectors). Simulated curves labeled "model" have been obtained from Eqs. (2) to (5) with n =2 and I_0 = 100 $m^{-2}.s^{-1}.sr^{-1}$.

Figure 10. Muon flux intensity as a function of the zenithal inclination angle measured in the East direction (full dots). The best fitting curve for the raw measurements is obtained for I_0 = 100 μ $m^{-2}.s^{-1}.sr^{-1}$ and n = 2.0 (full line).

Figure 11. Averaged values of the telescope counting rate as a function of both azimuthal (0 to 360°) and zenithal angles (0 to 90°). Each point corresponds to a value averaged over one hour. North direction has azimuth 0°, east 90°, south 180°, and west 270°; vertical direction has zenithal 0° and horizontal 90°. The radial scale shows the counting rate of the telescope.

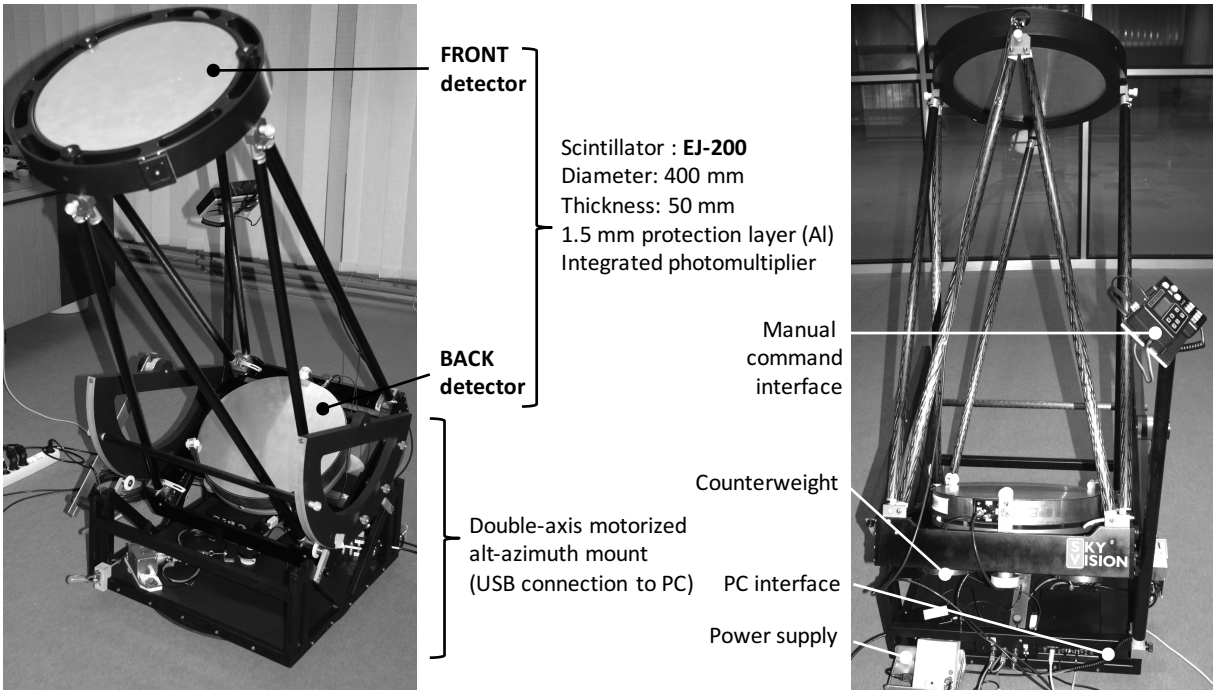

Autran et al. Figure 1

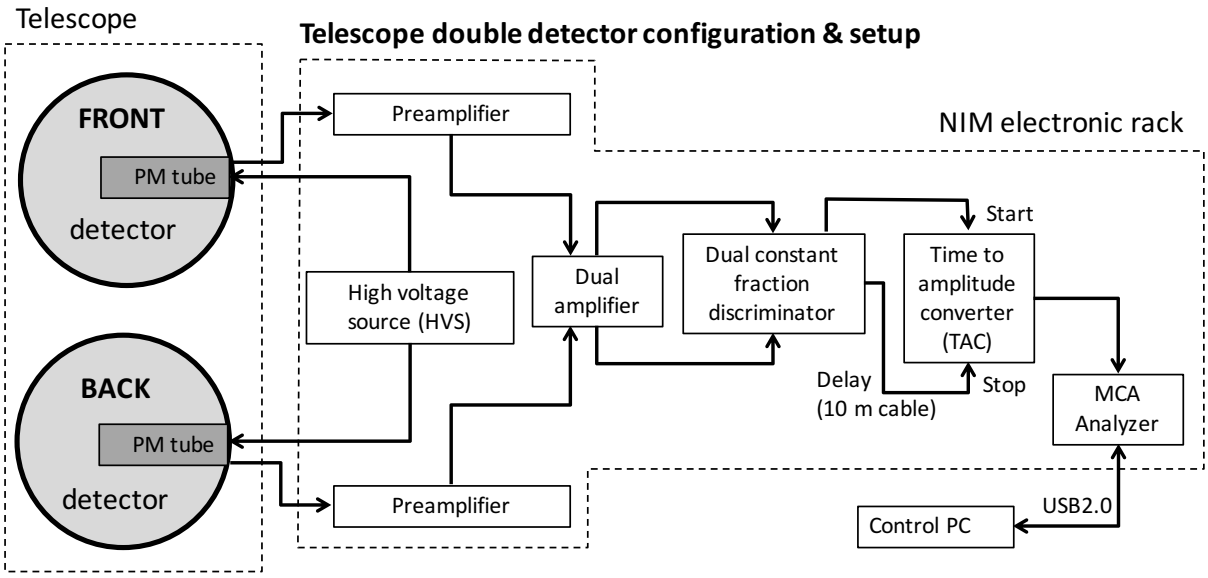

Autran et al. Figure 2

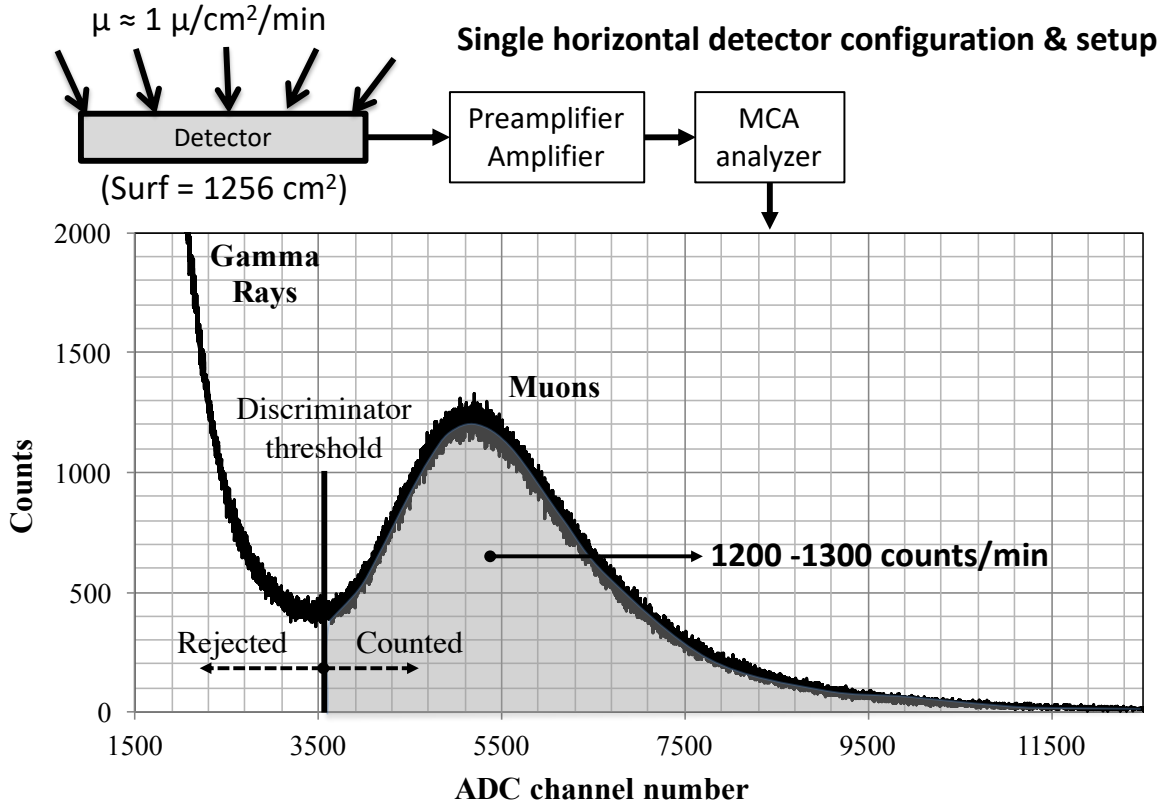

Autran et al. Figure 3

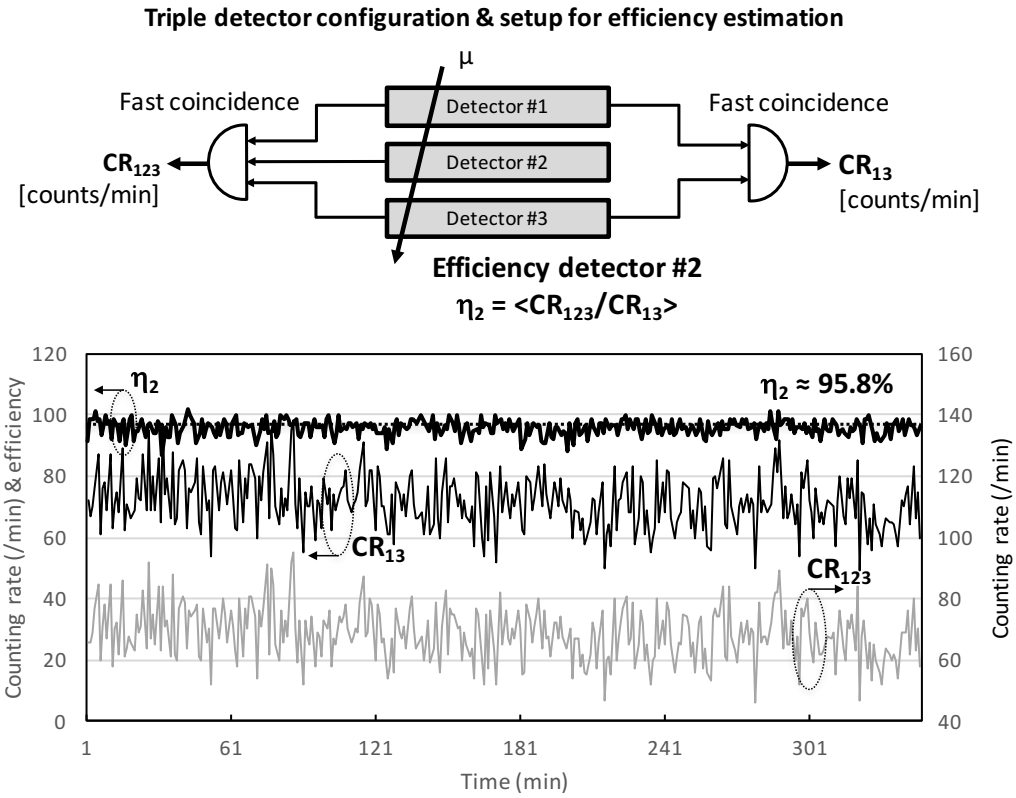

Autran et al. Figure 4

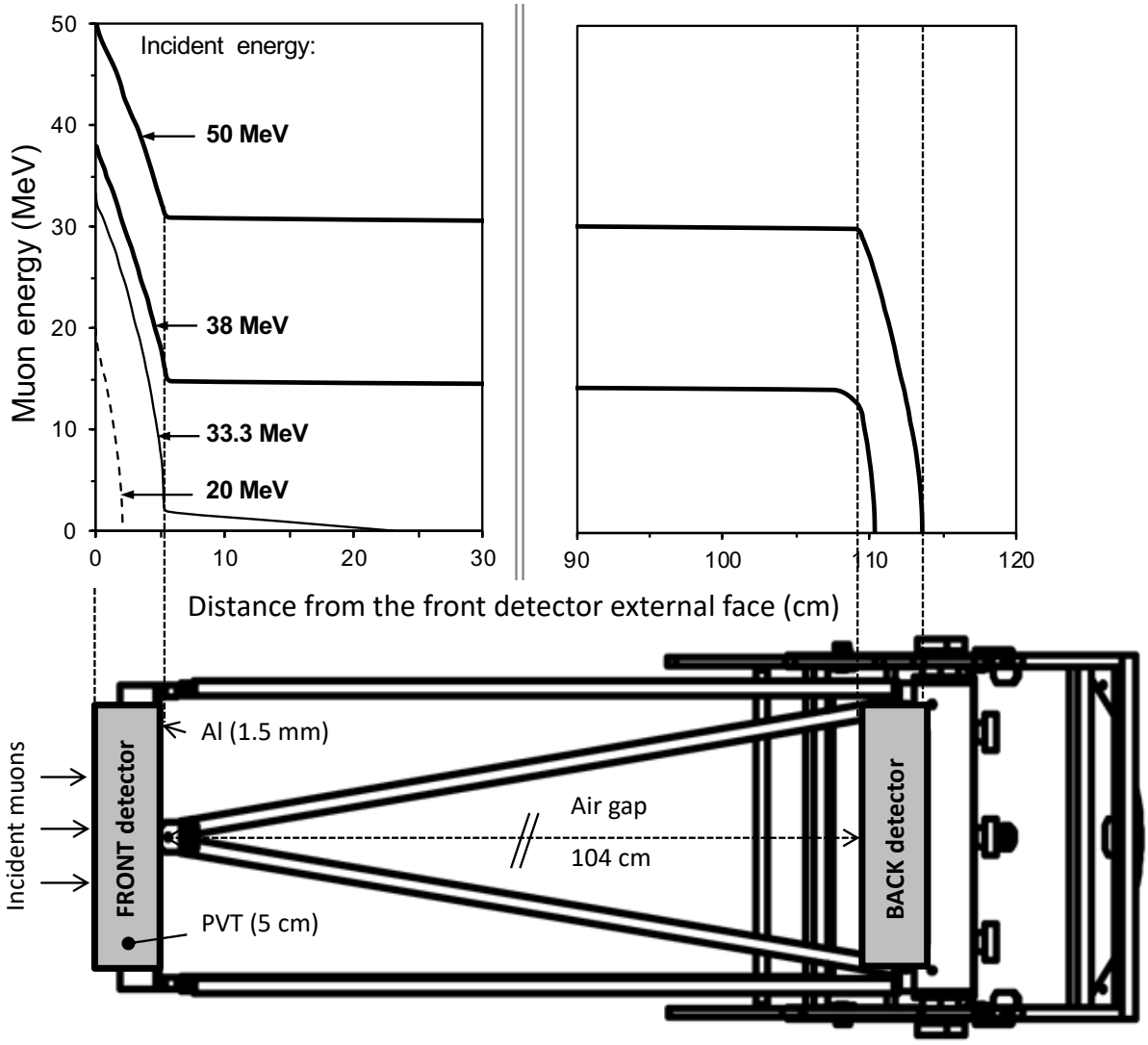

Autran et al. Figure 5

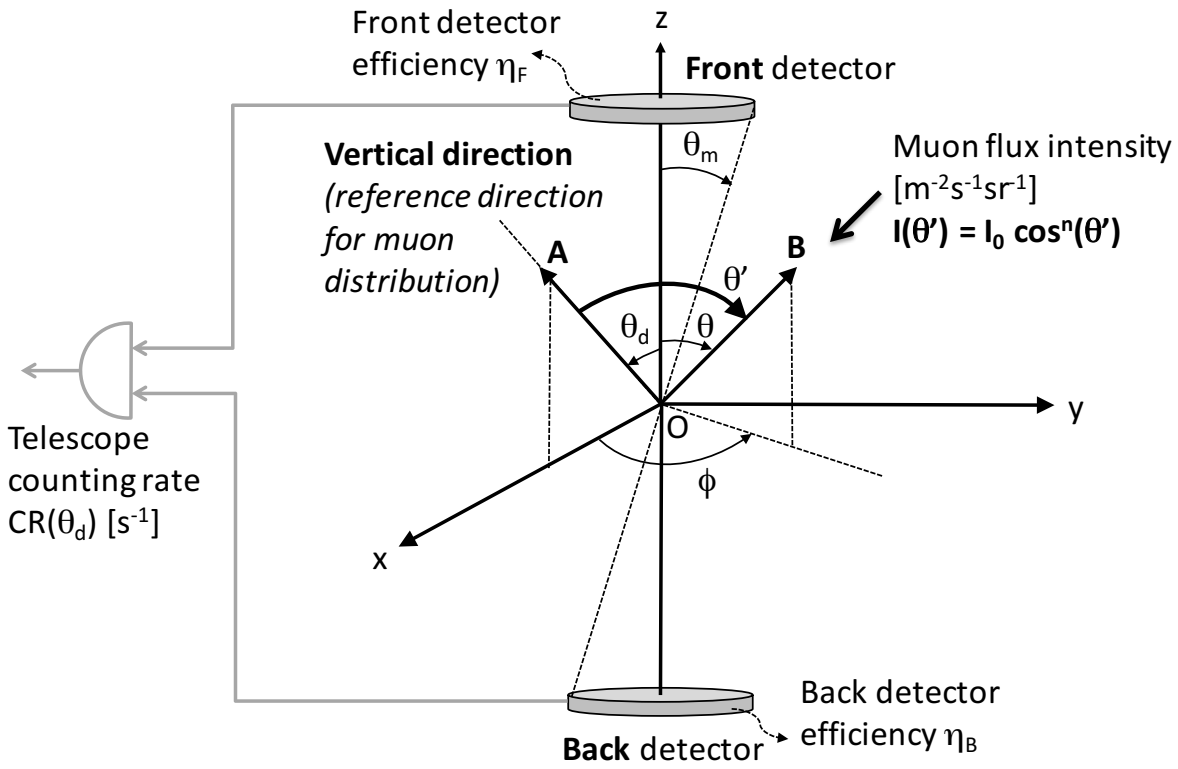

Autran et al. Figure 6

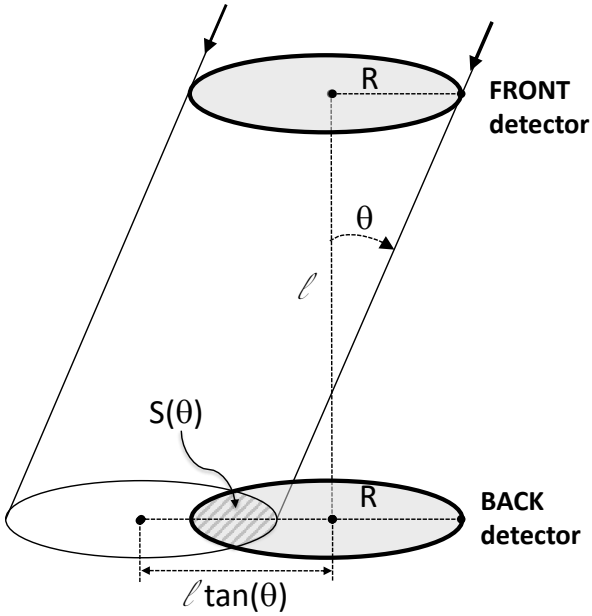

Autran et al. Figure 7

Autran et al. Figure 8

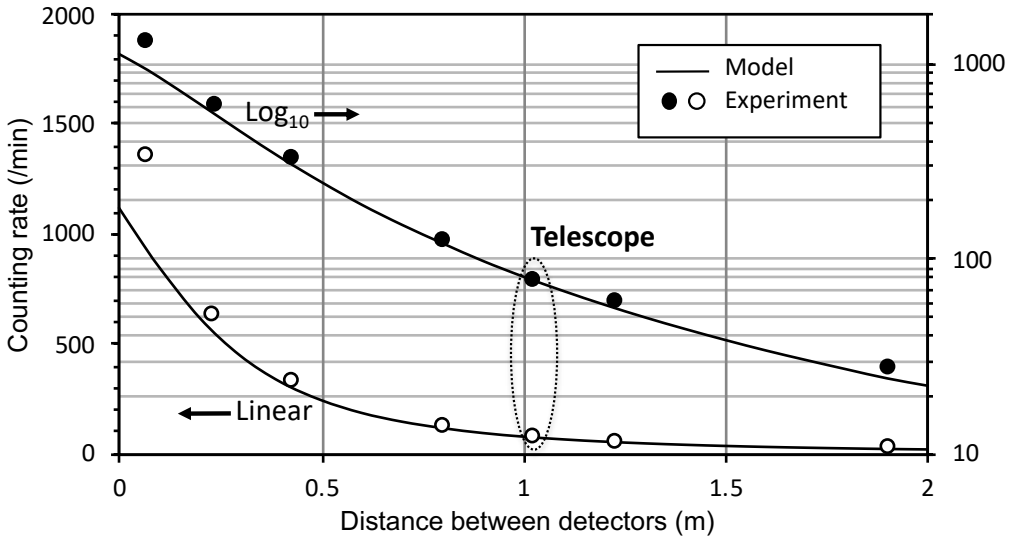

Autran et al. Figure 9

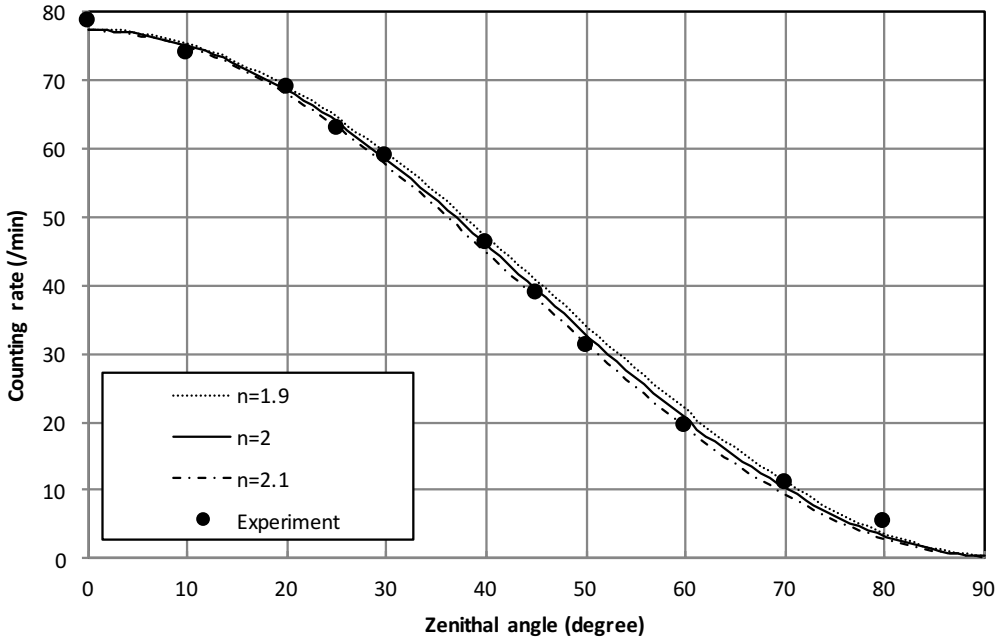

Autran et al. Figure 10

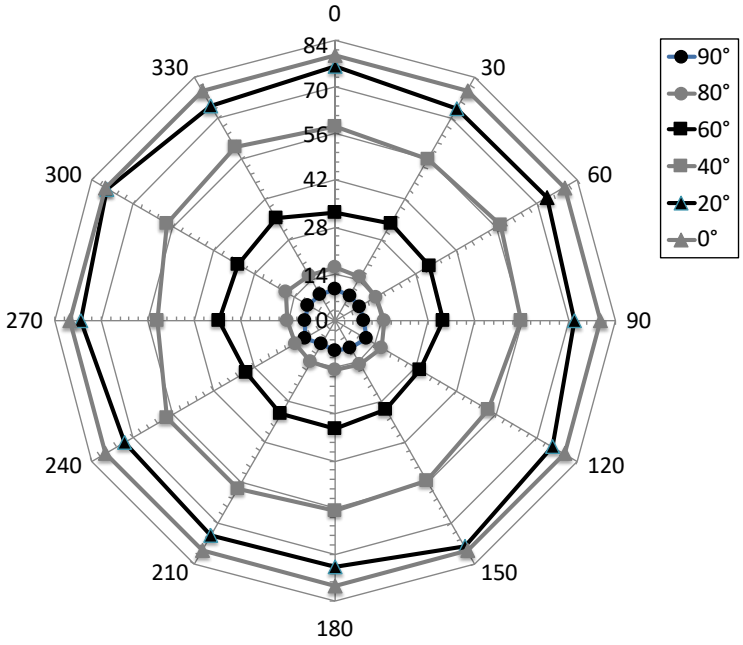

Autran et al. Figure 11